Output Regulation of Piezoelectric Tube Actuated Flexible Optical Fiber Using the Port Hamiltonian Framework ⋆

Mario Vargas *, **Yongxin Wu** *, **Yann Le Gorrec** **, **Kanty Rabenorosoa** *, **Alessandro Macchelli** ***

* *Universidad Regional Autonoma de los Andes, Via Banos Km 5 1/2, Uniandes Amboto Ecuador (email: ua.mariovb40@uniandes.edu.ec)*
** *Université Marie et Louis Pasteur, SUPMICROTECH, CNRS, institut FEMTO-ST, F-25000, Besançon, France,(emails: yongxin.wu, rkanty, yann.le.gorrec@femto-st.fr).*
*** *Department of Electrical, Electronic, and Information Engineering (DEI), University of Bologna, viale del Risorgimento 2, Bologna, Italy, (alessandro.macchelli@unibo.it)*

Abstract: This work introduces a port Hamiltonian system approach for an optical fiber actuated in two perpendicular directions using a piezoelectric tube, achieving desired periodic trajectories in both directions. The dynamics of the piezo tube actuator are represented by a finite-dimensional system, while the optical fiber is represented by an infinite-dimensional one. Additionally, the actuator and optical fiber are interconnected in a power-preserving manner. A control method for output regulation is proposed for the interconnected system, utilizing the internal model principle. The stability analysis of the closed-loop systems is also investigated. The proposed control method is validated through numerical simulations, demonstrating its effectiveness.

Keywords: port Hamiltonian system, output regulation, distributed parameter systems, optical fibre, piezo tube actuator.

1. INTRODUCTION

This paper aims to deal with the output regulation problem of the piezo tube-actuated optical fiber for the potential scanning application. Considering the multi-physical character of the scanning optical fiber and the large deformation, high flexibility and nonlinear characteristics of the motion of the optical fiber, the modelling of such kind of system is quite challenging. The port Hamiltonian (PH) formalism is particularly well-adapted for the modelling and the control of multi-physical systems (Duindam et al., 2009). The PH approach is based on the principle of conservation of energy and provides a clear physical interpretation of control design strategies. This approach, initially proposed in the context of finite-dimensional systems, was generalized to infinite-dimensional systems described by partial differential equations (PDEs) in (van der Schaft and Maschke, 2002). Moreover, the distributed PH formalism has been proven to be a powerful tool for the modelling, analyzing and control design for flexible structures, and several control techniques have been developed, see (Macchelli and Melchiorri, 2004). In Ayala et al. (2022), the Cosserat's rod model has been employed,the port Hamiltonian formulation for modelling the optical fiber and also established an interconnection and damping assignment passivity-based control. However, in this work, only the stabilization problem is addressed and the output tracking problem is not considered.

Over the past two decades, pioneering work has been conducted on the output regulation for infinite-dimensional systems (Rebarber and Weiss, 2003), including 1-D heat equations (Deutscher, 2015), beam equations (Jin and Guo, 2019), and wave equations (Guo et al., 2018). More recently, (Paunonen et al., 2021) investigated robust output tracking and disturbance rejection for a class of linear port Hamiltonian systems equipped with boundary control where the controller design is based on the internal model principle. In this paper, we present the first attempt to implement an output tracking controller on a finite-dimensional approximation of the nonlinear distributed port Hamiltonian system.

The paper is organized as follows. The representation of the optical fiber with the Cosserat rod model and its discretization is presented, together with the the interconnected system with the piezo tube actuator is given in Section 2. In Section 3, an output regulation control scheme to achieve trajectory tracking of an external periodical signal of the interconnected system is proposed and the stability proof of the closed-loop system is given using the Lyapunov method. Section 4 shows the numerical simulation results with real-world parameters to illustrate

⋆ This project has been supported by the EIPHI Graduate School (contract "ANR-17-EURE-0002"), by the Horizon Europe research and innovative programme under the Marie Sklodowska-Curie Actions (MSCA) grant agreement No. 101073558 (ModConFlex).

the effectiveness of the proposed controller. Finally, the conclusion and perspective of this work are presented in 5.

2. PORT HAMILTONIAN MODELING OF PIEZO-TUBE ACTUATED OPTIC FIBER

In this section, we present the PH model of an optical fiber actuated by a piezo tube. At first, the optical fiber is described by a Cosserat rod model (Till et al., 2019) within the PH framework. Additionally, the piezo-tube actuator is modeled as a finite-dimensional PH system which is interconnected to the optical fiber in a power-conserving way.

2.1 PH representation for the optical fiber

In this work, the optical fiber is considered as a slender rod which is approximated as a one dimensional beam under classical Cosserat's elastic assumption, (Rucker and III, 2011). The rod of length L is characterized by its centerline curve $p(s,t) \in \mathbb{R}^3$ and its material orientation $\Phi(s,t) \in SO(3)$ as functions of the arc length $s \in [0\ L]$ and time t. The complete set of PDEs describing the dynamic behavior of the Cosserat rod and the way they are derived can be found in (Till et al., 2019), (Rucker and III, 2011). We summarize and adopt the Cosserat rod model by equations (1) [1] , [2]

$$\begin{cases} p_s = \Phi v; \quad \Phi_s = \Phi \hat{u} \\ n_s = \rho A \Phi(\hat{w} q + q_t) - f \\ m_s = \rho \Phi(\hat{\omega}\mathcal{I}\omega + \mathcal{I}\omega_t) - \hat{p}_s n - l \\ q_s = v_t - \hat{u} q + \hat{\omega} v \\ \omega_s = u_t - \hat{u}\omega. \end{cases} \tag{1}$$

The partial derivative of p with respect to the arc length s in the local frame is denoted by v, that is $v = \Phi^T p_s$. In the same way, the local frame curvature is denoted by $u = (\Phi^T \Phi_s)^\vee$ where the operator $(\cdot)^\vee$ maps from $\mathfrak{so}(3)$ to $\mathbb{R}^3$ (Murray et al., 1994). The internal force and internal momentum are noted as n and m. The operator $(\cdot)^\wedge$ or $\hat{\ }$ maps from $\mathbb{R}^3$ to $\mathfrak{so}(3)$, *e.g.:*

$$\hat{u} = \begin{bmatrix} 0 & -u_3 & u_2 \\ u_3 & 0 & -u_1 \\ -u_2 & u_1 & 0 \end{bmatrix},$$

while $q = \Phi^T p_t$ and $\omega = (\Phi^T \Phi_t)^\vee$ are the velocity and angular velocity in the local frame. The terms f and l are the distributed force and moment acting on the rod. The physical parameters are the material density ρ, the cross sectional area A, the second mass moment of inertia tensor $\mathcal{I}$. The linear elastic laws with material damping are chosen as the material constitutive laws:

$$\begin{aligned} n &= \Phi\left[K_{se}(v - v^*) + B_{se} v_t\right], \\ m &= \Phi\left[K_{bt}(u - u^*) + B_{bt} u_t\right] \end{aligned} \tag{2}$$

where the "se" subscript stands for shear and extension and "bt" stands for bending and torsion. Besides, v^* stands for the initial state of the shear and axial elongation, and u^* represents the initial bending and torsion (curvature). In this work, we suppose that the initial position of the optical fiber is a straight rod, which implies that $v^* = (0,0,1)^T$ and $u^* = (0,0,0)^T$. The matrices $K_{se}, K_{bt} \in \mathbb{R}^{3\times3}$ are the stiffness matrix for shear and extension, and for bending and twisting, respectively, while B_{se}, $B_{bt} \in \mathbb{R}^{3\times3}$ are the Kelvin-Voigt type viscous damping matrices which depend on the material properties and cross-sectional geometry. More details can be found in (Linn et al., 2013).

Now, the goal is to derive a PH formulation of the optical fiber rod based on the Cosserat's rod dynamics (1) and on a proper definition of the energy. For that purpose we choose as state variables, the energy variables *i.e.* the extensive variables of Thermodynamics. The first energy variable is the difference of shear and axial elongation between the original and deformed states as in (3), while the second one is the internal translational momentum of the rod that depends on the cross-sectional area A and the linear velocity q of the material as in (4):

$$x_1 = v - v^*, \tag{3}$$

$$x_2 = \rho A p_t = \rho A q. \tag{4}$$

The third state variable is the difference in bending and torsion (curvature) between the original and deformed states of the rod as in (5). Finally, the fourth energy variable is the internal rotational momentum of the rod that is related to the inertia $\mathcal{I}$ and the angular velocity ω as in (6):

$$x_3 = u - u^*, \tag{5}$$

$$x_4 = \rho \mathcal{I} \Phi_t = \rho \mathcal{I} \omega. \tag{6}$$

The total energy is the sum of the potential elastic energy and kinetic energy of the rod. The potential elastic energy relates (3) with the shear and extension stiffness matrix K_{se}, and (5) with the bending and torsion stiffness matrix K_{bt}. The kinetic energy, which includes the internal translational and rotational momentum of the rod, depends on (4) and (6). Thus, the total energy (Hamiltonian function) is expressed as:

$$\mathcal{H}(x) = \frac{1}{2} \int_0^L x^T \mathcal{L} x \, ds \tag{7}$$

with $x = (x_1, x_2, x_3, x_4)^T$ and $\mathcal{L} = \text{diag}\left[K_{se}\ \frac{1}{\rho A}\ K_{bt}\ \frac{1}{\rho \mathcal{I}}\right]$.

The co-energy variables e are defined by the variational derivative of the Hamiltonian with respect to x, namely $e = \delta_x \mathcal{H}(x) = \mathcal{L} x$. The first co-energy variable is related to the shear and the elongation of the rod x_1 and is the force on the local frame (8). The second co-energy variable is related to the internal translational momentum x_2 and is the local velocity, as shown in (9):

$$e_1 = K_{se} x_1 = K_{se}(v - v^*), \tag{8}$$

$$e_2 = \frac{1}{\rho A} x_2 = \frac{1}{\rho A} \rho A q = q. \tag{9}$$

The third co-energy variable (10) is related with the bending and torsion. In the same way, the last co-energy variable in (11) is related to the internal rotational momentum:

$$e_3 = K_{bt} x_3 = K_{bt}(u - u^*), \tag{10}$$

$$e_4 = (\rho \mathcal{I})^{-1} x_4 = (\rho \mathcal{I})^{-1} \rho \mathcal{I} \omega = \omega. \tag{11}$$

The Cosserat's rod model with distributed input can be written in the PH framework as in van der Schaft (2020):

$$\begin{aligned} \dot{x} &= (J - R)\delta_x \mathcal{H}(x) + g u_d \\ y_d &= g^T \delta_x \mathcal{H}(x) \end{aligned} \tag{12}$$

where x is the state variable and $\delta_x \mathcal{H}(x) = \mathcal{L} x$ is the co-energy variable. The input $u_d = [f\ l]^T$ collects the

[1] For the sake of simplicity, the spatial and time variables (s,t) are omitted over the paper unless it causes confusion.

[2] p_s and p_t stand for the partial derivative of p with respect to the arc length $\frac{\partial p}{\partial s}$ and with respect to time $\frac{\partial p}{\partial t}$, respectively.

distributed force and momentum, and $J = \mathcal{J}_{lin} + J_{nl}$ is a formally skew-symmetric operator

$$J = \underbrace{\begin{bmatrix} 0 & \frac{\partial}{\partial s} & 0 & 0 \\ \frac{\partial}{\partial s} & 0 & 0 & 0 \\ 0 & 0 & 0 & \frac{\partial}{\partial s} \\ 0 & 0 & \frac{\partial}{\partial s} & 0 \end{bmatrix}}_{\mathcal{J}_{lin}} + \underbrace{\begin{bmatrix} 0 & \hat{u} & 0 & \hat{v} \\ \hat{u} & -\rho A\hat{\omega} & 0 & 0 \\ 0 & 0 & 0 & \hat{u} \\ \hat{v} & 0 & \hat{u} & -\rho\mathcal{I}\hat{\omega} \end{bmatrix}}_{J_{nl}}. \tag{13}$$

In fact, the operator $\mathcal{J}_{lin}$ is skew-symmetric when the boundary variables are chosen such as in (Le Gorrec et al., 2005), while the matrix J_{nl} is skew-symmetric since $\hat{u}, \hat{\omega} \in \mathfrak{so}(3)$ are skew-symmetric and ρ, A and $\mathcal{I}$ are constant. The dissipation matrix $R = R^T \geq 0$ and the input map g are defined as

$$R = \begin{bmatrix} 0 & 0 & 0 & 0 \\ 0 & B_{se} & 0 & 0 \\ 0 & 0 & 0 & 0 \\ 0 & 0 & 0 & B_{bt} \end{bmatrix} \quad g = \begin{bmatrix} 0 & 0 \\ \mathcal{I}^T & 0 \\ 0 & 0 \\ 0 & \mathcal{I}^T \end{bmatrix}. \tag{14}$$

Finally, the output $y_d = g^T \delta_x \mathcal{H}(x)$ is the power conjugate variable of the input u_d, *i.e.*, $y_d = \begin{bmatrix} \mathcal{I}^T q & \mathcal{I}^T \omega \end{bmatrix}^T$.

The boundary port variables of the PH model (12) are the co-energy variables evaluated in $s = 0$ and $s = L$. In this paper, the optical fiber rod is clamped to the piezo tube which leads to a clamped-free boundary condition with the velocity input on the clamped side in $s = 0$. From the boundary conditions, one can define the boundary input of the rod as

$$u_b = [e_2(0), e_4(0), e_1(L), e_3(L)]^T \tag{15}$$

i.e. velocity and angular velocity at the clamped side ($s = 0$) and the force and moment at the free side ($s = L$). The boundary output are chosen as the power conjugated boundary port variables, *i.e.:*

$$y_b = [e_1(0), -e_3(0), -e_2(L), e_4(L)]^T. \tag{16}$$

For more details on the parametrization of the boundary variables, the readers can refer to Le Gorrec et al. (2005). In this work, the optical fiber is controlled through the piezo tube motion acting on its boundary conditions. In this case, the distributed force and moment acting on the rod are equal to zero, *i.e.* $u_d = 0$.

2.2 Structure preserving discretization

In this paper, we consider the output-tracking control design based on the discretized version of PH Cosserat rod model (12). To this end, we employ the discretization method presented in (Trenchant et al., 2018) which preserves the PH structure.

In the discretized model, the state variables are collected into the $x_d = [x_d^1 \; x_d^2 \; x_d^3 \; x_d^4]^T \in \mathbb{R}^{(4\times 3)\times n}$, where the discrete energy variables are defined as $x_d^i = [x_1^i \dots x_n^i]^T$, with $i = 1, 2, 3, 4$. Here, the x_k^i with $k = 1, \dots, n$, are the approximations of the i-th state variable evaluated at each difference finite grid with length h. Similarly, e_0^2, e_0^4, e_{n+1}^1 and e_{n+1}^3 denote the boundary conditions at the clamped base and at the free tip of the rod. The vector of discretized co-energy variables is defined as $e_d = \mathcal{L}_d x_d$. This leads to the finite-dimensional PM system

$$\begin{bmatrix} \dot{x}_d^1 \\ \dot{x}_d^2 \\ \dot{x}_d^3 \\ \dot{x}_d^4 \end{bmatrix} = \Bigg[\underbrace{\begin{bmatrix} 0 & D & 0 & 0 \\ -D^T & 0 & 0 & 0 \\ 0 & 0 & 0 & D \\ 0 & 0 & -D^T & 0 \end{bmatrix} + \begin{bmatrix} 0 & \hat{u} & 0 & \hat{v} \\ \hat{u} & -\rho A\hat{\omega} & 0 & 0 \\ 0 & 0 & 0 & \hat{u} \\ \hat{v} & 0 & \hat{u} & -\rho\mathcal{I}\hat{\omega} \end{bmatrix}}_{J_d} - \underbrace{\begin{bmatrix} 0 & 0 & 0 & 0 \\ 0 & B_{se} & 0 & 0 \\ 0 & 0 & 0 & 0 \\ 0 & 0 & 0 & B_{bt} \end{bmatrix}}_{R_d} \Bigg] \underbrace{\begin{bmatrix} e_d^1 \\ e_d^2 \\ e_d^3 \\ e_d^4 \end{bmatrix}}_{e_d} + \underbrace{\frac{1}{h}\begin{bmatrix} g_1 \\ g_2 \\ g_3 \\ g_4 \end{bmatrix}}_{g_d} \underbrace{\begin{bmatrix} e_0^2 \\ e_{n+1}^1 \\ e_0^4 \\ e_{n+1}^3 \end{bmatrix}}_{u}; \tag{17}$$

$$\begin{bmatrix} y_1 \\ y_2 \\ y_3 \\ y_4 \end{bmatrix} = g^T \frac{\partial \mathcal{H}}{\partial x} = \frac{1}{h}\begin{bmatrix} g_1^T & g_2^T & g_3^T & g_4^T \end{bmatrix} \begin{bmatrix} e_d^1 \\ e_d^2 \\ e_d^3 \\ e_d^4 \end{bmatrix}$$

with

$$g_1 = \begin{bmatrix} -1 \\ 0 \\ \vdots \\ 0 \end{bmatrix} \quad g_2 = \begin{bmatrix} 0 \\ 0 \\ \vdots \\ 1 \end{bmatrix} \quad g_3 = \begin{bmatrix} -1 \\ 0 \\ \vdots \\ 0 \end{bmatrix} \quad g_4 = \begin{bmatrix} 0 \\ 0 \\ \vdots \\ 1 \end{bmatrix},$$

and D the discretised version of the partial derivative operator, *i.e.:*

$$D = \frac{1}{h}\begin{bmatrix} 1 & & & \\ -1 & 1 & & \\ & \ddots & \ddots & \\ & & -1 & 1 \end{bmatrix}. \tag{18}$$

To conclude, the discretized energy function of the rod is

$$\mathcal{H}_d(x_d) = \frac{1}{2} x_d^T \mathcal{L}_d x_d. \tag{19}$$

The discretization scheme has been presented in (Ayala et al., 2022) where the readers can find further details.

2.3 Port Hamiltonian formulation of the piezo tube

For control design purposes and simplicity, the piezo tube actuator described by a spring-mass-damper system. A voltage-dependent force $F_{pzt}(\mathrm{V})$ is applied to generate a displacement of the mass M of the actuator that is also subject to the restoring force from the rod $F_{rod} = e_0^1$. A stiffness K and a damper B are employed to cope with the piezo tube dynamics. Similarly to the the optical fiber, the model is written within the PH framework. The energy variables are the relative position p_{pzt} of the actuator and the momentum m_{pzt5pt}, defined in (20):

$$x_{p1} = p_{pzt}, \quad x_{p2} = m_{pzt}. \tag{20}$$

The Hamiltonian function is the sum of the potential and kinetic energies, *i.e.:*

$$\mathcal{H}_{pzt} = \frac{1}{2}\left[K x_{p1}^2 + \frac{1}{M} x_{p2}^2\right] = \frac{1}{2}\left[K p_{pzt}^2 + \frac{1}{M} m_{pzt}^2\right]. \tag{21}$$

and co-energy variables are

$$\begin{bmatrix} e_{p1} \\ e_{p2} \end{bmatrix} = \nabla \mathcal{H}_{pzt}(x_{pzt}) = \begin{bmatrix} K & 0 \\ 0 & \frac{1}{M} \end{bmatrix} \begin{bmatrix} x_{p1} \\ x_{p2} \end{bmatrix}. \tag{22}$$

Remark 1. In this work, we consider the piezo tube actuation on the $x-$ and $y-$ axes are independent. Hence, the piezo tube dynamics can be modeled by two spring-mass-damper systems and the energy variables of the piezo tube are denoted by $x_{p1}, x_{p2} \in \mathbb{R}^2$.

The piezo tube actuator PH model reads

$$\begin{cases} \dot{x}_{pzt} = (J_{pzt} - R_{pzt})\, e_{pzt} + g_{pzt} u_{pzt} + g_{pzt} u_{rod} \\ y_{pzt} = g_{pzt}^T e_{pzt} \end{cases} \tag{23}$$

with

$$J_{pzt} = \begin{bmatrix} 0 & I \\ -I & 0 \end{bmatrix} \quad R_{pzt} = \begin{bmatrix} 0 & 0 \\ 0 & b \end{bmatrix} \quad g_{pzt} = \begin{bmatrix} 0 \\ I \end{bmatrix}, \tag{24}$$

and where $b \in \mathbb{R}^{2\times 2}$ is the damper matrix and I is the 2×2 identity matrix. The input $u_{pzt} = F(V) \in \mathbb{R}^2$ collects the forces generated by the applied voltage on the piezo tube in $x-$ and $y-$ direction, while u_{rod} are the restoring forces exerted by the rod at the clamped point ($s = 0$) in the two directions. The output of the system are the velocities of the piezo tube, which are also the boundary inputs of the optical fiber, *i.e.*, e_0^2. The interconnection between the piezo tube (23) and the discretized optical fiber rod (17) is described by

$$\begin{bmatrix} e_0^2 \\ u_{rod} \end{bmatrix} = \begin{bmatrix} 0 & I \\ -I & 0 \end{bmatrix} \begin{bmatrix} e_0^1 \\ y_{rod} \end{bmatrix}. \tag{25}$$

Finally, because of the above interconnection law, the finite-dimensional model of the overall system reads:

$$\dot{x}_t = (\mathcal{J}_t - R_t) Q_t x_t + B u_t \tag{26}$$

where $x_t = \begin{bmatrix} x_{rod} \\ x_{pzt} \end{bmatrix}$, $u_t = u_{pzt}$, and the interconnection and damping matrices are defined as

$$\mathcal{J}_t - R_t = \left[\begin{array}{c|c} (J_d - R_d) & \mathcal{Z} \\ \hline \mathcal{C} & (J_{pzt} - R_{pzt}) \end{array}\right]$$

with

$$\mathcal{Z} = \frac{1}{h} \begin{bmatrix} g_1 & 0 \\ 0 & 0 \\ 0 & 0 \\ 0 & 0 \end{bmatrix} \qquad \mathcal{C} = \frac{1}{h} \begin{bmatrix} -g_1^T & 0 & 0 & 0 \\ 0 & 0 & 0 & 0 \end{bmatrix}.$$

The Hamiltonian function is

$$\begin{aligned} \mathcal{H}_t(x_t) = \frac{1}{2} \Big[& K_{se}(v - v^*)^2 + \rho A q^2 + K_{bt}(u - u^*)^2 \\ & + \rho \mathcal{I} \omega^2 + K p_{pzt}^2 + \frac{1}{M} m_{pzt}^2 \Big] = \frac{1}{2} x_t^T Q_t x_t \end{aligned} \tag{27}$$

and the input vector is $B = [0\ 0\ 0\ 0\ 0\ 1]^T$.

3. OUTPUT REGULATION CONTROL DESIGN

The control objective is to control the end tip of the optical fiber in the $x-$ and $y-$ directions by acting on the piezo tube. It is noticed that the position of interest is on the free boundary of the rod, which is different from the boundary condition where the piezo-tube and the rod are linked. As shown in Fig. 1, the variable y_m represents the output variable that we want to regulate. We define the desired trajectory of the end tip of optical fiber as y_d, so y_d is a

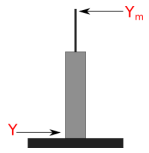

Fig. 1. Non-collocated output y_m.

vector that groups the desired output for rod and piezo tube. We assume that y_d is a periodical signal in the form

$$y_d = a_0 + \sum_{k=1}^{q} \left[a_k^1 \cos(w_k t) + a_k^2 \sin(w_k t) \right] \tag{28}$$

where w_k are the known signal frequency, $\{a_k^1\},\ \{a_k^2\} \subset \mathbb{R}^2$ are the unknown amplitudes. For this case $y_m(t) \in \mathbb{R}^2$ is the end tip displacement of the optical fiber in both $x-$ and $y-$ directions which are known as the non collocated outputs and can be seen as

$$y_m(t) = B_m^T Q_t x_t. \tag{29}$$

The error dynamics is defined as the difference between the desired trajectory and end tip position of the optical fiber $e = y_d - y_m$. We aim to find a control law such that

$$\lim_{t=\infty} ||y_d - y_m(t)|| = 0 \tag{30}$$

3.1 Controller structure

To achieve the control objective, we adopt the same structure of the controller presented in (Paunonen et al., 2021) and developed for linear distributed-parameter port Hamiltonian systems. Here, the plant (26) is a nonlinear discretized port Hamiltonian system, where the nonlinearity appears in the $\mathcal{J}_t$ term. To apply the controller proposed in (Paunonen et al., 2021), we separate the system (26) into linear and nonlinear parts, namely $\mathcal{J}_t = J_t + J_{nL}$. The controller takes the following form:

$$\begin{cases} \dot{x}_c = J_c x_c + \delta_c B_c e \\ y_c = \delta_c B_c^T x_c + D_c e \end{cases} \tag{31}$$

where $e = y_d - y_m$ is the error, δ_c is a tuning parameter and $D_c \geq 0$ is a constant that modifies the coupling between input and output. Note that, in a similar way as in (Paunonen et al., 2021), we let $D_c = 0$. The terms in the controller are defined as

$$J_c = \text{diagbloc}\ \begin{bmatrix} J_c^0 & J_c^1 & \cdots & J_c \end{bmatrix} \tag{32}$$

$$J_c^0 = [0\ 0] \quad J_c^k = \begin{bmatrix} 0 & w_k I_2 \\ -w_k I_2 & 0 \end{bmatrix} \tag{33}$$

$$B_c = \begin{bmatrix} B_c^0 \\ B_c^1 \\ \vdots \\ B_c^q \end{bmatrix} \quad B_c^0 = I_2 \quad B_c^k = \begin{bmatrix} I_2 \\ 0 \end{bmatrix} \tag{34}$$

If the controller is interconnected to the plant (26) so that $u_t = y_c$ and $e = y_d - y_m = y_d - B_m Q_t x_t$, the closed-loop system turns out to be

$$\begin{bmatrix} \dot{x}_t \\ \dot{x}_c \end{bmatrix} = \underbrace{\begin{bmatrix} J_t - R_t & \delta_c B B_c^T \\ -\delta_c B_c B_m^T & J_c \end{bmatrix}}_{\mathcal{A}_{cl}} \begin{bmatrix} Q_t x_t \\ x_c \end{bmatrix} + \begin{bmatrix} 0 \\ \delta_c \end{bmatrix} y_d \tag{35}$$

Thus, based on (Paunonen et al., 2021, Theorem IV.2), if the closed loop system (35) is stable, then it achieves the

output regulation objective (30) and the controller ensures that the output follows the desired reference (28).

3.2 Stability analysis

The closed-loop system (35) shares similarities with the one analyzed in (Paunonen et al., 2021). However, since the tracked output is not power-conjugated to the input, the closed-loop system does not arise from a power-conserving interconnection between the plant and the controller, and therefore, it does not exhibit a port-Hamiltonian (PH) structure. Consequently, the stability results established in (Paunonen et al., 2021) cannot be directly applied. Thus, the stability of the closed loop system (35) should be analyzed. To do so, we first consider the stability of linear part of closed loop system. Moreover, the nonlinear term J_{nL} is treated as a perturbation of the linear part in (35), whose stability is analyzed in the next Proposition.

Proposition 1. Let $0 = w_0 < w_1 < \ldots < w_q$ and assume that the linear part of (26) is exponentially stable. Then, the closed-loop system (35) in which the controller (31) is such that $J_c^T = -J_c$, $D_c = 0$ and $\delta_c > 0$ sufficient small is exponentially stable. Besides, the regulation error satisfies

$$\lim_{t=\infty} ||y_d - y_m(t)|| = 0 \tag{36}$$

Proof. Due to the fact that the linear part of open-loop system (26) is exponentially stable, there exists a Lyapunov function $V_1(x_t)$ such that

$$\begin{aligned} m x_t^T x_t < V_1(x_t) < M x_t^T x_t \\ \dot{V}_1(x_t) < -\gamma x_t^T x_t \end{aligned} \tag{37}$$

with $\gamma > 0$ and $M > m > 0$. To prove the stability in closed-loop, we propose the following Lyapunov function:

$$V(x_t, x_c) = nV_1(x_t) + \underbrace{\frac{1}{2} x_c^T x_c + x_t^T P B B_c^T x_c}_{V_2(x_t, x_c)} \tag{38}$$

with $P = P^T$. It is easy to show that there exists $M_V > m_V > 0$ such that $m_V < V(x_t, x_c) < M_V$, and this implies that V is a Lyapunov function candidate. Without loss of genearality, to simplify the computations, we let $Q_t = I$. This can be always obtained by coordinate transformation since Q_t is positive defined and full rank. Besides, we let $F_t = J_t - R_t$. The time derivative of $V_2(x_t, x_c)$ is

$$\begin{aligned} \dot{V}_2 &= x_c^T \dot{x}_c + x_t^T P B B_c^T \dot{x}_c + x_c^T B_c B^T P \dot{x}_t \\ &= x_c^T \left(-\delta_c B_c B_m^T x_t + J_c x_c\right) \\ &\quad + x_t^T P B B_c^T \left(-\delta_c B_c B_m^T x_t + J_c x_c\right) \\ &\quad + x_c^T B_c B^T P \left(F_t x + \delta_c B B_c^T x_c\right) \\ &= x_c^T J_c x_c - \delta_c x_c^T B_c B_m^T x_t - \delta_c x_t^T P B B_c^T B_c B_m^T x_t \\ &\quad + x_t^T P B B_c^T J_c x_c + \delta_c x_c^T B_c B^T P B B_c^T x_c \\ &\quad + x_c^T B_c B^T P F_t x_t \end{aligned} \tag{39}$$

Since $J_c = -J_c^T$ and by applying the Young's inequality $fg \leq \frac{1}{2\alpha} f^2 + \frac{\alpha}{2} g^2$ with $\alpha > 0$, we obtain

$$\begin{aligned} \dot{V}_2 \leq\ & \tfrac{\delta_c \alpha_1}{2} x_c^T B_c B_c^T x_c + \tfrac{\delta_c}{2\alpha_1} x_t^T B_m B_m^T x_t \\ & + \tfrac{\delta_c \alpha_2}{2} x_c^T J_c^T B_c B_c^T J_c x_c + \tfrac{\delta_c}{2\alpha_2} x_t^T P B B^T P x_t \\ & + \tfrac{\alpha_3}{2} x_c^T B_c B_c^T x_c + \tfrac{1}{2\alpha_3} x_t^T F_t^T P B B^T P F_T x_t \\ & + \delta_c x_c^T B_c B^T P B B_c^T x_c - \delta_c x_t^T P B B_c^T B_c B_m^T x_t \end{aligned} \tag{40}$$

Then we group all the terms containing x_c (i.e., the 1st, 3rd, 5th, and 7th terms) together and similarly collect the remaining terms involving x_t. The inequality (40) becomes:

$$\begin{aligned} \dot{V}_2 \leq\ & x_c^T \big(\delta_c B_c B^T P B B_c^T + \tfrac{\delta_c \alpha_1}{2} B_c B_c^T \\ & + \tfrac{\delta_c \alpha_2}{2} J_c^T B_c B_c^T J_c + \tfrac{\alpha_3}{2} B_c B_c^T\big) x_c \\ & + x_t^T \Big(\tfrac{\delta_c}{2\alpha_1} B_m B_m^T + \tfrac{\delta_c}{2\alpha_2} P B B^T P \\ & + \tfrac{1}{2\alpha_3} F_t^T P B B^T P F_t^T + \delta_c P B B_c^T B_c B_m^T\Big) x_t. \end{aligned} \tag{41}$$

If we choose $P = P^T < 0$, $\alpha_1 > 0$, $\alpha_2 > 0$, $\alpha_3 > 0$ and α_1, α_2, $\alpha_3$are sufficient small, then we can get the first term containing x_c in the last inequality is bounded by

$$\dot{V}_2(x_c) < -\gamma_1 x_c^T x_c \tag{42}$$

with $\gamma_1 > 0$. If we choose δ_c sufficient small and n sufficient large, then we can bound the second term of $\dot{V}_2(x)$ of inequality (41) by $n\dot{V}_1(x)$ such that

$$n\dot{V}_1(x_t) + \dot{V}_2(x_t) < -\gamma_2 x_t^T x_t \tag{43}$$

with $\gamma_2 > 0$.

Then we have

$$\begin{aligned} \dot{V}(x, x_c) &= n\dot{V}_1(x) + \dot{V}_2(x) + \dot{V}_2(x_c) \\ &< -\gamma_2 x_t^T x_t - \gamma_1 x_c^T x_c < \gamma_3 x^T x. \end{aligned} \tag{44}$$

where $\gamma_3 = \min\{\gamma_1, \gamma_2\}$ and $x = \begin{bmatrix} x_t \\ x_c \end{bmatrix}$. Then we can get the closed loop system (35) is exponentially stable. Furthermore, by applying (Paunonen et al., 2021, Theorem IV.2), if the closed loop system (35), we can get that the regulation error satisfies

$$\lim_{t=\infty} ||y_d - y_m(t)|| = 0 \tag{45}$$

which completes the proof.

Remark 1. To analyze the stability of the overall closed loop system (35), we consider the nonlinear term J_{nL} as a perturbation of the linear part of (35) and it is skew-symmetric. Since the parameter n in Lyapunov function (38) can be chosen sufficient large, then the nonlinear term $||J_{nL}||$ can be vanished as a perturbation (Khalil, 2002) which implies the closed loop stability.

4. SIMULATION VALIDATIONS

In this section, we will demonstrate the effectiveness of the proposed controller by numerical simulations. The parameters used to carry the simulation is given by the Table. 1, which is obtained from the experimental setup in FEMTO-ST.

Parameter	Value	Units
Fiber length (L)	0.03	m
Young's modulus of fiber(E)	9	GPa
Radius of fiber (r)	126	μm
Density of fiber (ρ)	1930	kg/m^3
Piezo tube stiffness (K)	27.5713	N/m
Piezo tube damping (b)	0.2821	Ns/m
Input force factor	0.7557	V/N

Table 1.

To carry out the simulation, we define the desired references on $X-$ and $Y-$direction are defined as

$$\begin{aligned} y_{dx} &= 2 \times 10^{-5} \sin(w_1 + \pi), \\ y_{dy} &= 1 \times 10^{-5} \sin\left(w_2 + \tfrac{\pi}{2}\right). \end{aligned} \tag{46}$$

The above two figures of Figure 2 show the tracking results for the output tracking control for $X-$ and $Y-$direction, respectively. The bottom figure in Figure 2 show the tracking error for two direction. We can find that the end tip position of the fiber converges to the desired references and the tracking errors go to zero around 6 second. where $w_1 = 4\pi$ and $w_2 = 8\pi$. We can observe that the Figure 3

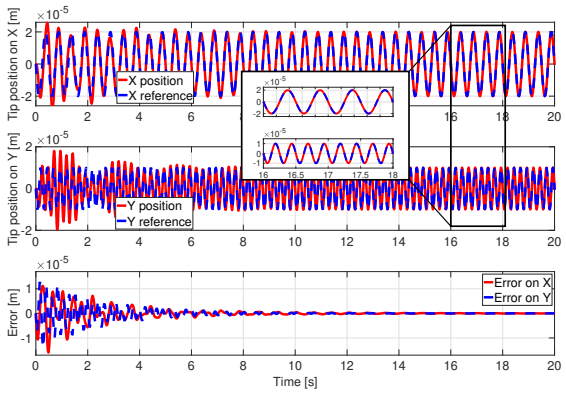

Fig. 2. Tip position tracking on X and Y

illustrates the tracking results in two dimensions and over time yielding the same outcome as the previous figure.

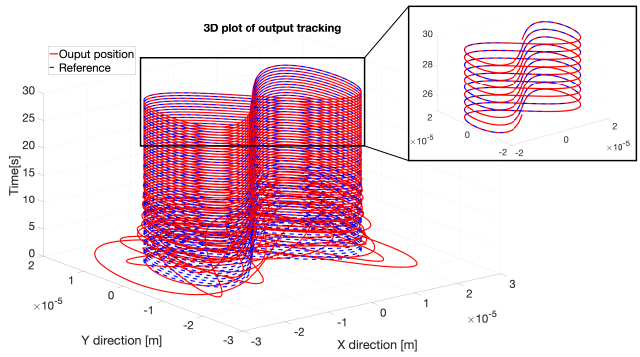

Fig. 3. Tip position tracking on 2D direction

5. CONCLUSION

In this paper, we address the output tracking problem for an optical fiber actuated by a piezoelectric tube in two perpendicular directions. The dynamics are modeled as a nonlinear distributed port Hamiltonian systemtransforming the control problem into a non-collocated output tracking problem. The resulting nonlinear distributed system is discretized in a structure preserving manner, and a control method for collocated output tracking in linear distributed port-Hamiltonian systems is adapted for this case. The exponential stability of the closed-loop system, along with the output tracking problem, is established using the Lyapunov approach. Numerical simulations with real-world parameters are conducted to demonstrate the effectiveness of the proposed controller.

For future work, further investigation into the well-posedness and stability proof of the closed-loop system for the nonlinear distributed port-Hamiltonian system is necessary. Additionally, experimental validation of the proposed control method should be pursued.

REFERENCES

Ayala, E.P., Wu, Y., Rabenorosoa, K., and Le Gorrec, Y. (2022). Energy-based modeling and control of a piezo-tube actuated optical fiber. *IEEE/ASME Transactions on Mechatronics*, 1–11.

Deutscher, J. (2015). A backstepping approach to the output regulation of boundary controlled parabolic PDEs. *Automatica*, 57, 56–64.

Duindam, V., Macchelli, A., Stramigioli, S., and Bruyninckx, H.e. (2009). *Modeling and Control of Complex Physical Systems - The Port-Hamiltonian Approach*. Springer.

Guo, W., Zhou, H.c., and Krstic, M. (2018). Adaptive error feedback regulation problem for 1D wave equation. *International Journal of Robust and Nonlinear Control*, 28(15), 4309–4329.

Jin, F.F. and Guo, B.Z. (2019). Boundary output tracking for an Euler–Bernoulli beam equation with unmatched perturbations from a known exosystem. *Automatica*, 109, 108507.

Khalil, H. (2002). *Nonlinear systems*. Prentice Hall.

Le Gorrec, Y., Zwart, H., and Maschke, B. (2005). Dirac structures and boundary control systems associated with skew-symmetric differential operators. *SIAM Journal on Control and Optimization*, 44(5), 1864–1892.

Linn, J., Lang, H., and Tuganov, A. (2013). Geometrically exact cosserat rods with Kelvin–Voigt type viscous damping. *Mechanical Sciences*, 4, 79–96.

Macchelli, A. and Melchiorri, C. (2004). Modeling and control of the timoshenko beam: The distributed port Hamiltonian approach. *SIAM Journal on Control and Optimization*, 43(2), 743–767.

Murray, R., Li, Z., Sastry, S., and Sastry, S. (1994). *A Mathematical Introduction to Robotic Manipulation*. Taylor & Francis.

Paunonen, L., Le Gorrec, Y., and Ramírez, H. (2021). A Lyapunov approach to robust regulation of distributed port–Hamiltonian systems. *IEEE Transactions on Automatic Control*, 66(12), 6041–6048.

Rebarber, R. and Weiss, G. (2003). Internal model based tracking and disturbance rejection for stable well-posed systems. *Automatica*, 39(9), 1555–1569.

Rucker, D.C. and III, R.J.W. (2011). Statics and dynamics of continuum robots with general tendon routing and external loading. *IEEE Transactions on Robotics*, 27(6), 1033–1044.

Till, J., Aloi, V., and Rucker, C. (2019). Real-time dynamics of soft and continuum robots based on Cosserat rod models. *The International Journal of Robotics Research*, 38(6), 723–746.

Trenchant, V., Ramirez, H., Le Gorrec, Y., and Kotyczka, P. (2018). Finite differences on staggered grids preserving the port-Hamiltonian structure with application to an acoustic duct. *Journal of Computational Physics*.

van der Schaft, A. and Maschke, B. (2002). Hamiltonian formulation of distributed parameter systems with boundary energy flow. *Journal of Geometry and Physics*, 42, 166–194.

van der Schaft, A. (2020). Port-Hamiltonian modeling for control. *Annual Review of Control, Robotics, and Autonomous Systems*.